CHINESE OPTICS LETTERS

Vol. 24, No. 6 | June 2026

Investigation of stable dual-pulse bunches in a Yb-doped mode-locked fiber laser at ultralow repetition rates using an NALM

Xue Cao (曹 雪)[1,2,3], Feng Li (李 峰)[1*], Jixin Xing (行纪欣)[1], Qianglong Li (李强龙)[1], Wenlong Wen (温文龙)[1], Lei Wang (王 磊)[1], Yufeng Wei (魏玉凤)[1], Yishan Wang (王屹山)[1**], Yuxi Fu (付玉喜)[1], Wei Zhao (赵 卫)[1], and Jinhai Si (司金海)[2]

[1] State Key Laboratory of Ultrafast Optical Science and Technology, Xi'an Institute of Optics and Precision Mechanics, Chinese Academy of Sciences, Xi'an 710119, China

[2] Key Laboratory for Physical Electronics and Devices of the Ministry of Education and Shaanxi Key Lab of Information Photonic Technique, School of Electronics and Information Engineering, Xi'an Jiaotong University, Xi'an 710049, China

[3] University of Chinese Academy of Sciences, Beijing 100049, China

*Corresponding author: lifeng@opt.ac.cn

**Corresponding author: yshwang@opt.ac.cn

Received October 10, 2025 | Accepted January 21, 2026 | Posted Online June 2, 2026

We numerically and experimentally investigate an all-normal dispersion (ANDi) Yb-doped mode-locked fiber laser that generates ultralow repetition rate dual-pulse bunches using a nonlinear amplifying loop mirror (NALM). The numerical simulation constructed specific cavity parameters and filtering effect to realize dual-pulse bunches evolution characteristics, which show a high consistency between the experimental results and numerical simulations. Specifically, through careful positioning of fiber sections in the cavity, we achieve stable dual-pulse bunches at repetition rates as low as 367 kHz with a 3 dB spectral width of 10.4 nm, which shows a wider spectral bandwidth at such low several hundred kilohertz repetition rate mode-locking lasers reported so far. To verify the compressibility of mode-locked pulses, the seed laser is amplified to 2.93 μJ and compressed using a grating pair. The mode-locked fiber laser can achieve a narrow-compressed pulse width below 300 fs. The laser shows excellent stability and environmental robustness in high-power fiber amplification for industrial applications.

Keywords: ultrafast fiber laser; mode-locking; amplifier.

© The Authors. Published by Chinese Laser Press under a Creative Commons Attribution 4.0 International License. Distribution or reproduction of this work in whole or in part requires full attribution of the original publication, including its DOI.

DOI: 10.3788/COL202624.061402

1. Introduction

Mode-locked fiber lasers (MLFLs) have gained significant attention due to their unique properties and versatility to generate high-quality ultrashort pulses[1–4]. They are now well-developed and have been encountered in widespread application fields including material processing and manufacturing[5,6], nonlinear optics[7], multiphoton imaging[8], and biological medicine[9]. Therefore, various mode-locking methods have been developed to improve the performance of oscillators. Compared with typical soliton MLFLs[10] and dispersion-managed MLFLs[11], the all-normal dispersion (ANDi) mode-locked fiber lasers with the output pulse described as dissipative solitons (DSs) achieve more attention due to their capability of generating higher-energy compressible pulses without the need for complex dispersion arrangements[12]. As a consequence, with the pump power higher than the threshold, the multi-pulse operation is always generated in the laser cavity and then numerically simulates the formation mechanisms by subsequent research[13,14]. The multi-pulse operation of ultrafast fiber lasers shows great significance for enormous applications such as extra-high-speed optical communication systems and femtosecond laser micromachining. Specifically, it shows better laser processing results in material ablation rates compared to the common single pulse[15–17].

Most ever reported ANDi lasers often show a pulse repetition rate (PRR) operating at 10–100 MHz, for cavity lengths less than 20 m, which is stable with considerably less optical nonlinearities[18,19]. However, applications such as micromachining and high-order harmonic generation necessitate a PRR less than 1 MHz for ultrashort pulses[20,21]. Specifically, in the case of obtaining the same high pulse energy, the ultralow-repetition-rate laser system shows much lower average power, which can substantially reduce the heat accumulation of the target material. Moreover, the approach to achieving such low PRR in an ultrafast laser system often employs external pulse pickers to reduce PRR from the seeder such as those reported lasers above. Nevertheless, laser systems employing these approaches suffer from several drawbacks: they hinder system integration, introduce additional inevitable losses, and increase both complexity and cost. Therefore, a stable source directly delivering ultralow repetition rates is preferred for a broad range of applications.

To date, many ultralow-repetition-rate ANDi mode-locked fiber lasers based on giant chirp oscillator (GCO) designs have been demonstrated in recent years. This design often shows temporally broad pulses and a very large linear chirp[22–24]. In addition, Renninger *et al.*[22] presented the theoretical properties of such a GCO design and reported a nonlinear polarization evolution (NPE) mode-locked laser operated at a repetition rate of 3 MHz with pulse spectral widths of 5 nm. In 2012, a 1.7 MHz giant chirp oscillator with pulse spectral widths of 12 nm based on an all-polarization-maintaining (PM) fiber nonlinear amplifying loop mirror (NALM) was demonstrated[25]. The laser was compressed to 370 fs, showing a pedestal contained with approximate 20% of pulse energy, which is due to the third-order dispersion accumulated in the ultralong fibers in the cavity. By carefully distributing the two long fiber sections in the main loop, stable pulse trains with spectral bandwidths of ~7 nm and compressed pulse duration of 500 fs at repetition rates as low as 506 kHz were demonstrated[26]. Then, a spectral width of 5.2 nm at 448 kHz was obtained by employing one section of long PM fiber in the main loop[27]. Through a single-mode amplifier, the pulse was further amplified to 134 nJ with a compressed pulse duration of 870 fs. In 2021, this group achieved pulse trains at the lowest repetition rate of 140 kHz with a spectral width of 4.5 nm and can be further amplified to 27 μJ by a three-stage cascaded amplifier with compressed pulse duration down to 1.16 ps[28]. In 2023, Stoliarov *et al.* explored the gain-managed nonlinear (GMN) amplification of ultralow-repetition-rate pulses in the range of 956 kHz[29]. Moreover, the spectrum of 31 nm with pulse energy of 10 nJ was demonstrated at a relatively high repetition rate of 6 MHz, and the pulses were compressed to 93 fs[30]. Further, the multi-pulse operation naturally occurs when the pump power is higher than a threshold. Considering the great significance for enormous applications of the multi-pulse operation of ultrafast fiber lasers, many multiple DS operations in the ANDi lasers were also experimentally researched. In 2021, Cao *et al.* reported triple DSs with pulse energy of 48.8 nJ at a repetition rate of 2.541 MHz[31]. Up to 30 pulses in the bunch coexisting in the ANDi fiber laser were demonstrated by enhancing the spectral filtering and adjusting the pump power[32].

Additionally, many efforts have also been made in the pursuit of achieving oscillators with lower repetition rates; however, their spectral widths were almost invariably very narrow (<1 nm), which makes it difficult to compress the pulse width to sub-picoseconds[33,34]. Therefore, realizing all-fiber ANDi lasers that emit stable pulse trains and simultaneously combine the advantages of broad spectral bandwidth (>10 nm), high pulse energy (>10 nJ), and short pulse duration (<300 fs) at low PRRs (<1 MHz) remains a challenging task.

In this paper, we investigate an all-PM, ANDi, mode-locked fiber laser that generates ultralow-repetition-rate (367 kHz) dual-pulse bunches with a spectral width of 10.4 nm. The MLFL can achieve the narrow-compressed pulse width below 300 fs. The simulation results illustrate that the performance of the fiber laser and pulse characteristics are significantly influenced by the intracavity parameter conditions, especially for a repetition rate below 1 MHz. According to the experimental condition, the numerical simulations are used to construct specific cavity parameters and a filtering effect to realize dual-pulse bunches evolution characteristics, which show a high consistency between the experimental results and numerical simulations. The source with excellent stability and environmental robustness can be beneficial for high-power fiber amplification used in industrial processing.

2. Numerical Simulations

Figure 1 shows the block diagram of the laser cavity for numerical simulation. The resonator is constructed by a typical figure-eight configuration and consists of two loops combined by a 2 × 2 coupler. In this work, we simulate each part of the laser cavity and list the specific cavity parameters used in the simulation in Table 1, where the five laser components are described in detail.

The generalized nonlinear Schrodinger equation (GNLSE) is used for the simulation of the optical pulse propagation in Yb-doped fiber (YDF):

$$\frac{\partial A(z,\tau)}{\partial z}+\frac{i}{2}\beta_2\frac{\partial^2 A(z,\tau)}{\partial \tau^2}-\frac{1}{6}\beta_3\frac{\partial^3 A(z,\tau)}{\partial \tau^3}=\frac{g}{2}A(z,\tau)+i\gamma\left(1+i\frac{1}{\omega_0}\frac{\partial}{\partial \tau}\right)\left(A(z,\tau)\int_0^{\infty}R(\tau_0)|A(z,\tau-\tau_0)|^2\mathrm{d}\tau_0\right),\quad(1)$$

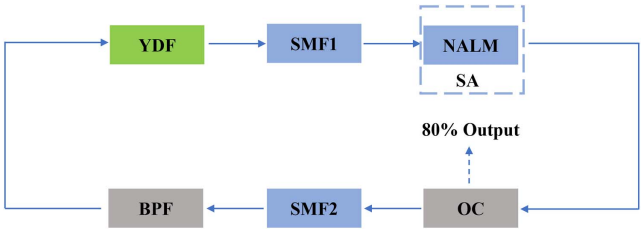

Fig. 1. Block diagram of the simulated laser cavity.

Table 1. Cavity Parameters in the Simulation.

YDF	SMF	OC	BPF	NALM
L_{YDF} = 2.4 m	β_2 = 20.2 ps^2/km	80% output	λ_{BW} = 1030 nm	ρ = 0.5
λ_0 = 1030 nm	β_3 = 0.037 ps^3/km		$\Delta\lambda_{BW}$ = 2 nm	L_{Loop} = 5 m
$\Delta\lambda_g$ = 40 nm	L_{SMF1} = 100 m		Order = 7	
g_0 = 30 dB/km	L_{SMF2} = 400 m			
P_{sat} = 29 dBm	γ = 4.7 m^{-1} kW^{-1}			

where $A(z,\tau)$ is the amplitude of the optical pulse envelope in the temporal domain with z as the propagation coordinate and τ as the time-delay parameter; β_2 and β_3 represent the group velocity dispersion (GVD) and third-order dispersion (TOD) coefficients at the center angular frequency ω_0, respectively; γ is the nonlinearity coefficient; $R(\tau_0)$ is the nonlinear response function; g is the spectrum-dependent coefficient of the gain fiber, which can be modeled by

$$g = g_0/(1 + E/E_{sat}). \tag{2}$$

g_0 is the small-signal gain coefficient, which accounts for the intrinsic loss of the Yb-doped fiber; E is the intracavity pulse energy and E_{sat} is the saturation energy related to pump power. In addition, $g = 0$ for the passive fibers.

The devices in the dashed box work as a virtual saturable absorber (SA) with the transmitted field of the input pulses divided into clockwise and counterclockwise propagations. To simulate the coupler in the NALM, we describe the model with the following equation:

$$A_{cw} = \sqrt{\rho}A_{in}, \quad A_{ccw} = i\sqrt{1-\rho}A_{in}, \tag{3}$$

where A_{cw} and A_{ccw} refer to the two light fields divided by the coupler; A_{in} is the incident light field amplitude and ρ is the coupler ratio. Then, according to Eq. (1), we simulated the two beams passing through the loop and the interference between these two anti-propagating fields occurs in the coupler. The output transmission field can be calculated as

$$A_{out} = \sqrt{\rho}A'_{cw} + i\sqrt{1-\rho}A'_{ccw}. \tag{4}$$

A'_{cw} and A'_{ccw} are the estimated amplitudes of the two light fields passing through a loop.

Combined with the block diagram shown in Fig. 1, we divide the laser components that affect pulse state distribution into five parts, which are gain fiber, passive fiber, output coupler (OC), bandpass filter (BPF), and NALM loop. As shown in Table 1, these five laser components are described by several corresponding parameters, among which the bandpass filter width $\Delta\lambda_{BW}$, fiber length L_{SMF1}, L_{SMF2}, L_{YDF}, gain saturation power P_{sat}, NALM loop length L_{Loop}, and coupler ratio ρ affect spectral filtering loss, nonlinearity, gain, and saturation absorption, respectively. The length of the first single-mode fiber (SMF) L_{SMF1} contributes to the intracavity intensity and the second SMF L_{SMF2} is located after the OC, reducing the accumulation of nonlinearities.

The bandpass filter (BPF) with a typical seven-order super-Gaussian profile centered at 1030 nm is applied to model the rectangular-shaped transmission spectrum of the filter. In order to be consistent with the subsequent experiments, the parameters of the bandpass filter and OC are set to the actual values. In our model, all components connected via PM SMF are regarded as having the same GVD. β_2 is 20.2 ps^2/km and nonlinearity coefficient γ is 4.7 m^{-1} kW^{-1}. Specifically, we simulate the pulse state distributions by controlling the above parameters in Table 1.

To accelerate the convergence of the calculation, the simulation starts from a combined light of Gaussian white noise and ~10 ps weak pulse with a spectrum wavelength centered at 1030 nm. The gain bandwidth $\Delta\lambda_g$ of the YDF is 40 nm with a Gaussian shape. Compared with the split-step Fourier method, we use a faster and more accurate interaction picture method in the frequency domain for numerical calculation in our simulation. Further, considering the optimization that enables automatic calculation of a large amount of pulse states in the simulation, we used the local error method and set the initial step size of 0.00001 km/step. After several roundtrips, the initial pulse propagates through each component in the cavity with roundtrip iterations until the light field converges to a steady-state solution.

Here, we simulate the pulse formation characteristics of the fiber laser that is significantly influenced by the intracavity parameter conditions. Specifically, the pulse state distributions are simulated by controlling the above parameters in Table 1. To study the evolution process of single-pulse and multi-pulse dynamics in the fiber laser, we achieve different mode-locking states by increasing the intracavity gain to enhance pump intensities. Figure 2 shows the pulse evolution of two mode-locked pulse states changing with different small-signal gain coefficients g_0. It can be seen that when we set g_0 as 20 dB/km, the output pulse is maintained in a single-pulse mode-locking state with 200 roundtrips, as shown in Fig. 2(a). However, when the g_0 is 28 dB/km and 29 dB/km, the laser system changes to unstable operation, with results shown in Fig. 2(b). In the case of unstable pulse operation, by increasing

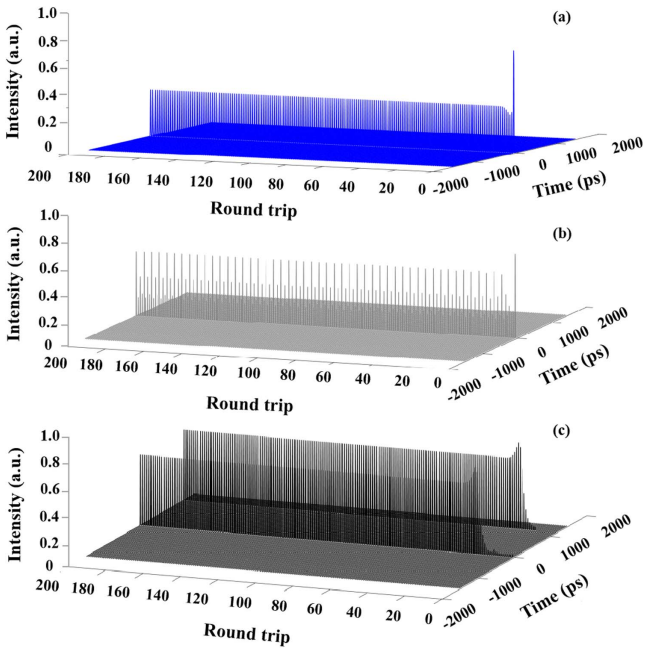

Fig. 2. The pulse evolution of two mode-locked pulse states changing with small-signal gain coefficient g_0. (a) g_0 = 20 dB/km; (b) g_0 = 28 dB/km; (c) g_0 = 30 dB/km.

the g_0 (equal to increasing pump power) to vary from 30 dB/km to 35 dB/km, the peak power of the mode-locked pulse reaches saturation and the fundamental mode-locked pulse begins to split, resulting in the generation of the dual-pulse bunches, as presented in Fig. 2(c). The interval between the two pulses remains at ~1.2 ns during the whole evolution process and the dual-pulse bunches can be stably maintained within a large adjustment range by increasing the intracavity gain. Moreover, the dual-pulse bunches exhibit the same pulse energy and remain constant along with the roundtrip for the energy quantization theory, a natural consequence of the gain competition between the solitons.

To directly observe the three mode-locked pulse states, Fig. 3 shows the spectral and pulse evolution process of these mode-locked pulse operations with two-dimensional evolution diagrams. From the above simulation, we can flexibly control the transition between different mode-locking states by adjusting the intracavity gain, that is, by increasing the pump power in the experiment.

As can be seen in Figs. 3(a) and 3(d), we get the spectral evolution with the spectral width of 6.4 nm centered at 1030 nm and pulse evolution with the autocorrelation curve of the single-pulse operation. By continuing to increase the pump power, we get the unstable operation at $g_0 = 28$ dB/km, shown in Figs. 3(b) and 3(e). The spectral shape clearly shows the modulation instability of linear waves during the evolution process. As we continued to elevate the intracavity gain, Fig. 3(c) shows the stable dual-pulse bunches mode-locked state in this all-PM fiber laser system with the spectrum bandwidth of ~10 nm. In these states, the dual-pulse bunches exhibit the same pulse amplitude and remain constant along with the roundtrip, with results shown in Fig. 3(f).

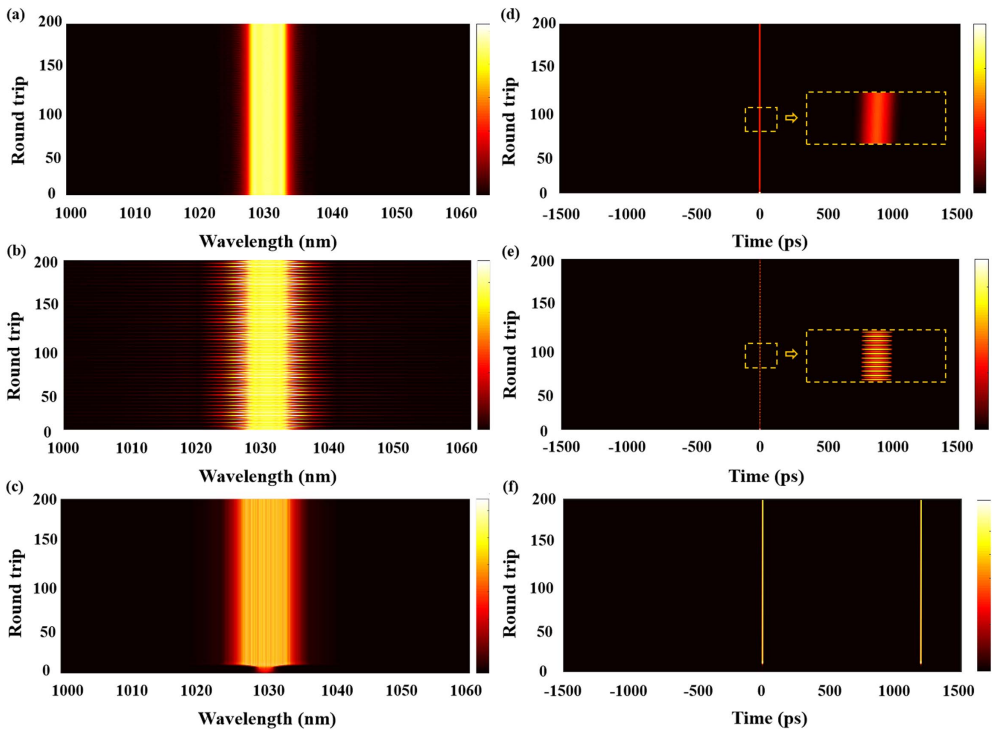

Fig. 3. The spectral and pulse evolution of three mode-locked pulse states changing with small-signal gain coefficient g_0. (a), (d) g_0 = 20 dB/km, single-pulse operation; (b), (e) g_0 = 28 dB/km, unstable pulse operation; (c), (f) g_0 = 30 dB/km, dual-pulse operation. Inset: the enlarged time domain pulse details.

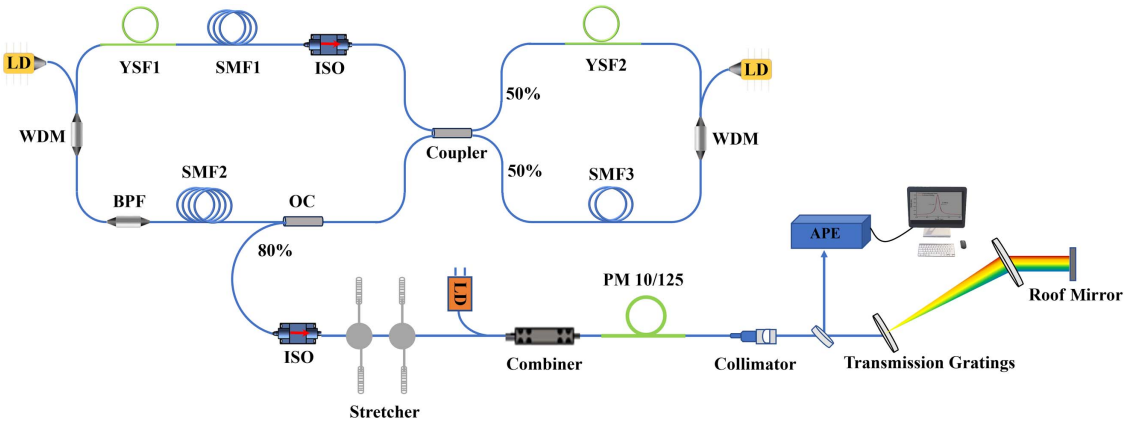

Fig. 4. Experimental setup of the laser system.

3. Experimental Results and Discussion

The schematic illustration for the all-PM mode-locked YDF laser with a figure-of-eight configuration is shown in Fig. 4. The laser cavity consists of a main unidirectional ring (UR) and an NALM acting as a saturable absorber (SA). Compared with the traditional saturable absorber, the NALM as a virtual saturable absorber can flexibly control the nonlinear transfer function and saturable absorption characteristics. In the main UR of the laser, up to several hundreds of meters of fiber are distributed in two spools at different positions that can overcome the nonlinear limitations and sustain much lower repetition rates. A 2.4 m long highly doped Yb fiber (Nufern PM-YSF-HI-HP) is pumped by a single-mode (SM) 974 nm laser diode (LD) via a wavelength division multiplexer (WDM). Unidirectional operation of the oscillation is ensured using a fiber isolator after the gain fiber. The output was taken from the 80% port by the following 20/80 coupler, while the 20% port continues to transmit in the cavity. A Gaussian-shaped narrow bandpass filter (BPF) centered at 1030 nm is inserted into the main UR to ensure the cavity's boundary conditions for suppressing the mode competition effect. The bidirectional NALM loop is constructed using a 50/50 coupler. It contains a short segment of PM SMF and a 1.2 m long gain fiber, the same as the main UR, which is pumped by an LD via another WDM. In our experimental setup, we set the two separately pumped gain sections for a flexible variable control of the mode-locked operation. The total ultra-long cavity length is achieved by carefully changing the length of the two SMF spools with all-normal dispersion and promoting stable dual-pulse bunches at repetition rates as low as several hundreds of kHz having a 3 dB spectral line width of ~10 nm. The tailed fibers of all components in the cavity are single-mode fiber (SMF) PM980-XP, ensuring the all-fiber configuration combines excellent advantages in terms of stability and integration. Then, we inject the seed laser pulse into the two cascaded stretchers with a GVD of ~87 ps/nm and 50 ps/nm. After the stretchers, the seed pulse is amplified through a 10/125 double cladding (DC) amplifier and then collimated into the compressor (a pair of 1600 lines/mm transmission gratings).

Three mode-locking Yb-doped NALM fiber lasers with repetition rates of 1.12 MHz, 587 kHz, and 367 kHz by carefully changing the length of the two SMF spools are demonstrated. In these three cases, the mode-locking states can be easily achieved by adjusting the pump power in the main UR as well as in the NALM loop; the detailed output characteristics are summarized in Table 2, where: f_{rep}, repetition rate in kHz; SMF1 and SMF2, lengths of spools 1 and 2 in m; P_M and P_N, pump powers of main and NALM loops in mW; P_{av}, output average power in mW; E, output pulse energy in nJ; $\Delta\lambda$, spectral width in nm; $\Delta\tau$, pulse duration in ps. The pulse energy of the three seeders exceeds 10 nJ, mainly due to the relatively low repetition rate and the two separately pumped gain sections for large gain in our cavity. Especially, the oscillator has repetition rates of 367 kHz; the table gives the parameters of two mode-locked states: the former parameter represents the single-pulse state, and the latter represents the dual-pulse bunches state. In addition, due to the fact that the output energy was taken from the 80% port by the coupler, while only 20% energy is left to

Table 2. Design Parameters and Output Characteristics for Different Laser Configurations.

f_{rep} (kHz)	SMF1 (m)	SMF2 (m)	P_M (mW)	P_N (mW)	P_{av} (mW)	E (nJ)	$\Delta\lambda$ (nm)	$\Delta\tau$ (ps)
1120	35	100	88	124	15	13.4	9	27
587	100	200	80	130	13	22.1	8.2	59
367	100	400	83/140	117/87	4/9	10.9/24.5	6.2/10.4	59/69

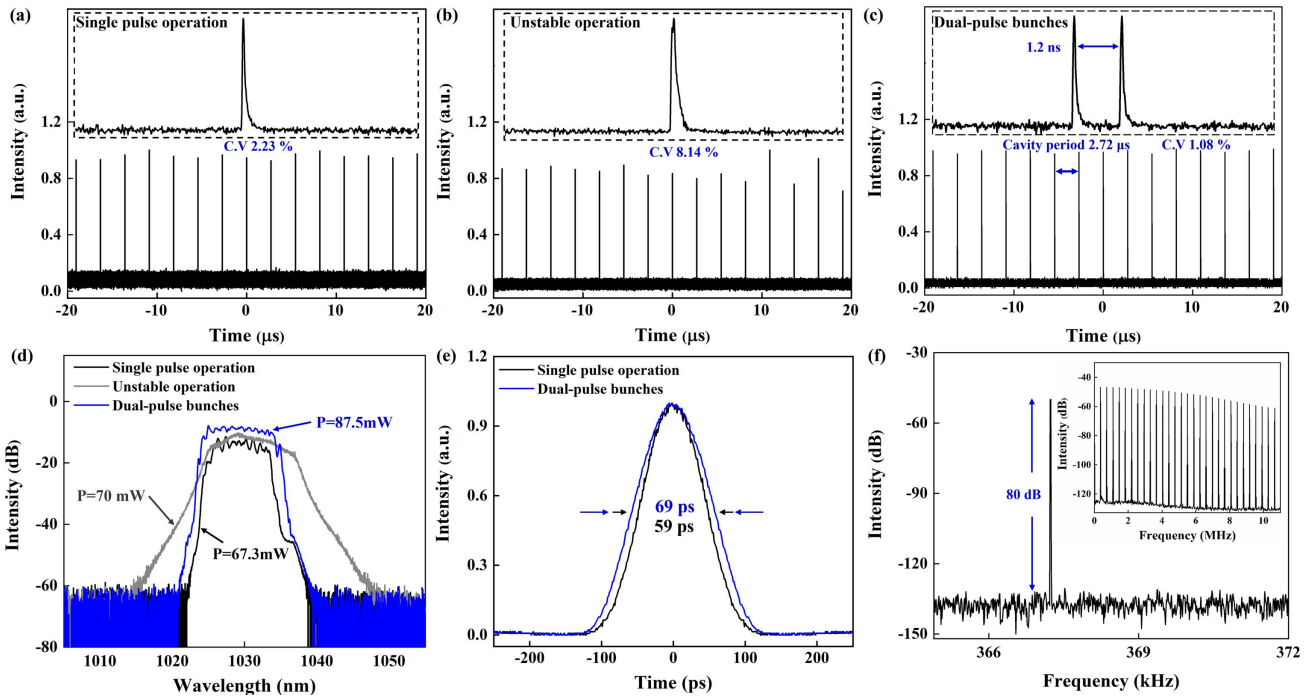

Fig. 5. Oscilloscope trace of single-pulse operation at pump power P = 67.3 mW (a), unstable mode-locking state at P = 70 mW (b), and dual-pulse bunches at P = 87.5 mW (c). Optical spectra (d) and autocorrelation traces (e) of different pulse states. RF spectrum of the dual-pulse bunches mode-locked pulse (f).

transmit in the cavity, the accumulation of nonlinearity in the cavity is greatly weakened. Therefore, while increasing the cavity length, the length of the passive fiber spool is placed as much as possible in the second segment of passive fiber spool SMF2 after the OC to avoid excessive nonlinear accumulation. In detail, 500 m of SMF was distributed in the two positions with 100 m of SMF1 and 400 m of SMF2 in the main UR; single-pulse and dual-pulse bunches are achieved in the ANDi Yb-doped fiber laser.

With the pump power of the main UR fixed at 140 mW, the single-pulse mode-locking state is maintained as the pump power in the NALM loop varies from 56.8 to 67.3 mW. Figure 5(a) shows the temporal characteristics of the obtained stable mode-locked single pulse in the 40 μs time scale and we calculate the coefficient of variation (C.V) of the amplitude intensity as 2.23%. The maximum optical spectrum bandwidth and the corresponding pulse duration are 6.2 nm [see Fig. 5(d)] and 59 ps [see Fig. 5(e)] at a pump power of 67.3 mW, respectively. However, when the pump power in the NALM loop varies from ~68 to ~72.8 mW, the laser changes to the unstable operation due to the modulation instability of linear waves together with the spectral filtering effect, and an unstable operation at a pump power of 70 mW is shown in Fig. 5(b). The relative instability pulse train shows the C.V of 8.14% and the spectrum also has many multiple spikes with the spectral bandwidth of 5 nm as shown in Fig. 5(d). By further increasing the pump power in the NALM loop to 87.5 mW, the stable dual-pulse bunches can be reached with a relatively small C.V of 1.08% due to the peak power clamping effect. The pulse-to-pulse interval of the pulse train is 2.72 μs, corresponding to the fundamental repetition frequency of 367.5 kHz as shown in Fig. 5(c). We measure the pulse train by the high-speed photodetector with a bandwidth of 45 GHz and an 80 GS/s digital oscilloscope, showing that the intensity of each of the dual-pulse bunches is nearly equal and the pulse-to-pulse interval in each pulse bunch is ~1.2 ns [see the inset of Fig. 5(c)]. The stable mode-locked optical spectrum bandwidth of ~10.4 nm is shown in Fig. 5(d). Besides, there is no modulation in the spectrum of the dual-pulse bunches, mainly due to the too large pulse-to-pulse interval to interact with each other compared with the bound-state pulses. The autocorrelation trace shows the pulse duration of 69 ps [see Fig. 5(e)] and we further measured the RF spectrum with results shown in Fig. 5(f), showing the SNR of the dual-pulse bunches mode-locked states exceeding 80 dB with the scan range of 10 kHz and resolution bandwidth (RBW) of 5 Hz. Figures 5(d) and 5(e) exhibit that the spectral width broadens and the pulse duration increases by enhancing the pump power.

To sum up, the parameters of the laser cavity exhibit a systematic and regular regulatory effect on the repetition rate, spectral width, and pulse duration. The repetition rate is inversely proportional to total cavity length. Spectral width is positively correlated with pump power and pulse energy, and can be enhanced by optimal cavity length and nonlinear management. Pulse duration from the oscillator increases with cavity length and dispersion, but the compressed pulse duration is inversely related to spectral width and depends on dispersion compensation quality.

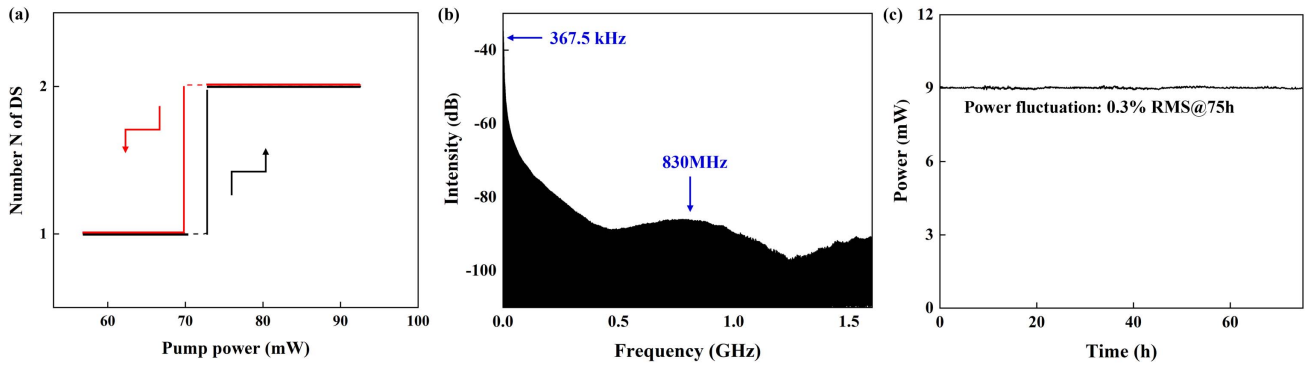

Fig. 6. (a) Pulse states as a function of the pump power. The solid and dashed lines denote the stable and unstable mode-locking states of the laser, respectively. The stepwise-up and stepwise-down curves refer to the ascending and descending pump-power processes, respectively. (b) RF spectrum with a scan range of 1.5 GHz. (c) Output power stability measurement.

Meanwhile, the establishment and annihilation of each mode-locked state is accompanied by the hysteresis phenomena when we adjust the pump power. As shown in Fig. 6(a), the pulse operation alternately evolves on the single-pulse and dual-pulse bunches mode-locking states as a function of the pump power. In the case of single-pulse operation, by increasing the pump power to a certain value, the peak power of the mode-locked pulse reaches saturation with the fundamental mode-locked pulse splitting and the generation of the dual-pulse bunches. The solid line denotes the stable mode-locking states of the laser. The unstable operation of the laser represented by the dashed line is due to the combined effects of the modulation instability of linear waves and the spectral filtering effect of the gain bandwidth. Figure 6(b) shows the RF spectrum with a scan range of 1.5 GHz and an RBW of 100 Hz. We observe that the RF spectrum has a periodic modulation envelope of 830 MHz, corresponding to the pulse-to-pulse interval in each pulse bunch of 1.2 ns. To verify the high quality of the dual-pulse bunches, the power fluctuation in 75 h continuously is monitored by a power meter (Ophir) with the output power of 9 mW and the root mean square (RMS) value was 0.3%, with results shown in Fig. 6(c).

To test the amplification capabilities of this homemade oscillator, we constructed an all-PM DC fiber amplifier. As shown in Fig. 7(a), we injected the dual-pulse bunches into the two cascaded stretchers with the GVD of ~87 ps/nm and 50 ps/nm and stretched the pulse width of 2.7 ns. The stretched pulse achieves sufficient pulse stretching before amplification, thereby mitigating nonlinear pulse distortion and avoiding optical damage in the gain fiber. After the stretchers, the seed pulse is amplified through a 10/125 amplifier pumped by a 9 W fiber coupled 976 nm multi-mode (MM) LD and then compressed by a pair of 1600 lines/mm transmission gratings, with the results shown in Fig. 7(b). At the pump power of 4.84 W, the maximum amplified power is 1.08 W with the slope efficiency of 49.15%; the corresponding pulse energy is 2.94 μJ. The measured compressed spectrum is shown in Fig. 7(c).

Considering the two cascaded stretchers with a GVD of ~87 ps/nm and 50 ps/nm, we carefully adjust the distance of the grating pair to match the GVD well. To precisely compensate for GVD, the laser pulse has a little bit of obvious filtration after a long distance of 2.4 m without affecting the effective compression of the main pulse. As shown in Fig. 8, the pump power increases from 1.28 to 4.84 W, while the compressed autocorrelation traces with a long scan scale of 50 ps vary from 228 to 517 fs. The compressed output power is 132 mW with the pump power of 1.28 W, and a pulse duration of 228 fs is obtained with a relatively smooth pulse profile

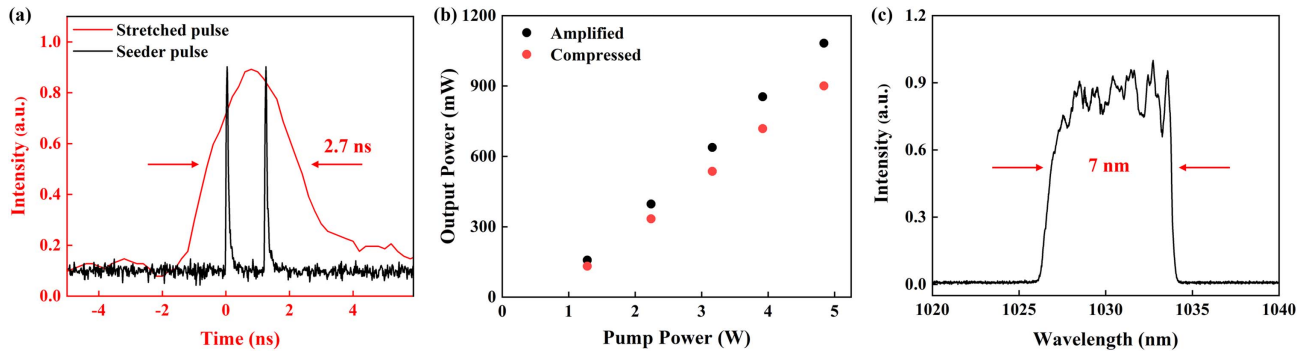

Fig. 7. (a) The stretched dual-pulse bunches with the pulse width of 2.7 ns. (b) The amplified and compressed output powers versus the pump power. (c) The compressed spectrum.

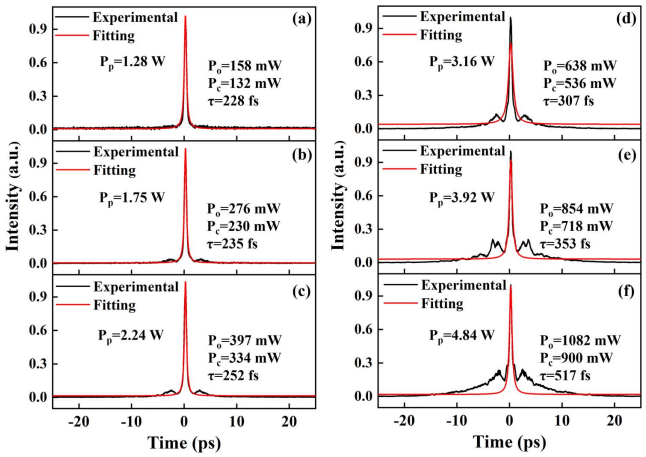

Fig. 8. The compressed autocorrelation traces with the pump power varying from 1.28 W to 4.84 W.

[see Fig. 8(a)]. Meanwhile, the compressed pulse curves at the pump power below 2.24 W are shown in Figs. 8(b) and 8(c), where the pulse energy is still concentrated at the main peak of the pulse envelope. However, as the pump intensity further increased, we find that the pulse has two small wings because of the accumulation of nonlinear effects [see Figs. 8(d)–8(f)]. The compressed pulse energy is about 2.45 μJ, corresponding to the peak power of 4.73 MW.

4. Conclusion

In summary, we have both theoretically and experimentally investigated the all-PM Yb-doped NALM dual-pulse bunches mode-locked laser with ultralow repetition rates ranging from 1.12 MHz to 367.5 kHz. Specifically, through careful positioning of fiber sections in the cavity, we achieve stable dual-pulse bunches at repetition rates as low as 367 kHz with a 3 dB spectral width of 10.4 nm and a pulse energy of 24.5 nJ. The output pulses are compressible down to ultrashort (<300 fs) durations with a grating pair compressor. Notably, the spectral width of 10.4 nm shows a wider spectral bandwidth at such low several hundred kilohertz repetition rate mode-locking lasers reported so far. Finally, we construct an all-PM DC fiber amplifier with the maximum amplified power of 1.08 W and the compressed pulse energy of 2.45 μJ. The entire laser system is very compact without using any pulse selector and multistage fiber preamplifier.

Acknowledgements

This work was supported by the National Key Research and Development Program of China (No. 2024YFB3613500), the Chinese Academy of Sciences "Light of West China" Program (No. XAB2021YN12), and the Independent Research Project of State Key Laboratory of Ultrafast Optical Science and Technology.

References

1. X. Huang, X. Guo, X. Huang, *et al.*, "Highly birefringence-guided microfiber resonator for ultra-high repetition rate ultrashort pulse," Laser Photonics Rev. **18**, 2400166 (2024).
2. Y. Song, Z. Wang, C. Wang, *et al.*, "Recent progress on optical rogue waves in fiber lasers: status, challenges, and perspectives," Adv. Photonics **2**, 024001 (2020).
3. C. Jauregui, J. Limpert, and A. Tünnermann, "High-power fibre lasers," Nat. Photonics **7**, 861 (2013).
4. J. Kim and Y. Song, "Ultralow-noise mode-locked fiber lasers and frequency combs: principles, status, and applications," Adv. Opt. Photonics **8**, 465 (2016).
5. K. C. Phillips, H. H. Gandhi, E. Mazur, *et al.*, "Ultrafast laser processing of materials: a review," Adv. Opt. Photonics **7**, 684 (2015).
6. K. Sugioka, Y. Cheng, and K. Midorikawa, "Three-dimensional micromachining of glass using femtosecond laser for lab-on-a-chip device manufacture," Appl. Phys. A **81**, 1 (2005).
7. A. Zach, M. Mohseni, C. Polzer, *et al.*, "All-fiber widely tunable ultrafast laser source for multimodal imaging in nonlinear microscopy," Opt. Lett. **44**, 5218 (2019).
8. B. Resan, R. Aviles-Espinosa, S. Kurmulis, *et al.*, "Two-photon fluorescence imaging with 30 fs laser system tunable around 1 micron," Opt. Express **22**, 16456 (2014).
9. K. Subramanian, I. Gabay, O. Ferhanoğlu, *et al.*, "Kagome fiber based ultrafast laser microsurgery probe delivering micro-Joule pulse energies," Biomed. Opt. Express **7**, 4639 (2016).
10. I. N. Duling III, "All-fiber ring soliton laser mode locked with a nonlinear mirror," Opt. Lett. **16**, 539 (1991).
11. K. Tamura and M. Nakazawa, "Optimizing power extraction in stretched-pulse fiber ring lasers," Appl. Phys. Lett. **67**, 3691 (1995).
12. P. Grelu and N. Akhmediev, "Dissipative solitons for mode-locked lasers," Nat. Photonics **6**, 84 (2012).
13. D. Tang, L. Zhao, B. Zhao, *et al.*, "Mechanism of multisoliton formation and soliton energy quantization in passively mode-locked fiber lasers," Phys. Rev. A **72**, 043816 (2005).
14. A. Komarov, H. Leblond, and F. Sanchez, "Multistability and hysteresis phenomena in passively mode-locked fiber lasers," Phys. Rev. A **71**, 053809 (2005).
15. A. Ancona, F. Röser, K. Rademaker, *et al.*, "High speed laser drilling of metals using a high repetition rate, high average power ultrafast fiber CPA system," Opt. Express **16**, 8958 (2008).
16. A. Nebel, T. Herrmann, B. Henrich, *et al.*, "Generation of tailored picosecond-pulse-trains for micro-machining," in *Commercial and Biomedical Applications of Ultrafast Lasers VI* (SPIE, 2006), p. 226.
17. R. Knappe, H. Haloui, A. Seifert, *et al.*, "Scaling ablation rates for picosecond lasers using burst micromachining," in *Laser-based Micro- and Nanopackaging and Assembly IV* (SPIE, 2010), p. 150.
18. H. Kalaycıoğlu, Y. Eldeniz, Ö. Akçaalan, *et al.*, "1 mJ pulse bursts from a Yb-doped fiber amplifier," Opt. Lett. **37**, 2586 (2012).
19. Z. Zhao and Y. Kobayashi, "Ytterbium fiber-based, 270 fs, 100 W chirped pulse amplification laser system with 1 MHz repetition rate," Appl. Phys. Express **9**, 012701 (2015).
20. S. M. Eaton, H. Zhang, P. R. Herman, *et al.*, "Heat accumulation effects in femtosecond laser-written waveguides with variable repetition rate," Opt. Express **13**, 4708 (2005).
21. C. L. Evans and X. S. Xie, "Coherent anti-Stokes Raman scattering microscopy: chemical imaging for biology and medicine," Annu. Rev. Anal. Chem. **1**, 883 (2008).
22. W. H. Renninger, A. Chong, and F. W. Wise, "Giant-chirp oscillators for short-pulse fiber amplifiers," Opt. Lett. **33**, 3025 (2008).
23. N. B. Chichkov, C. Hapke, K. Hausmann, *et al.*, "0.5 μJ pulses from a giant-chirp ytterbium fiber oscillator," Opt. Express **19**, 3647 (2011).
24. E. Kelleher and J. Travers, "Chirped pulse formation dynamics in ultra-long mode-locked fiber lasers," Opt. Lett. **39**, 1398 (2014).
25. M. Erkintalo, C. Aguergaray, A. Runge, *et al.*, "Environmentally stable all-PM all-fiber giant chirp oscillator," Opt. Express **20**, 22669 (2012).
26. P. Bowen, M. Erkintalo, R. Provo, *et al.*, "Mode-locked Yb-doped fiber laser emitting broadband pulses at ultralow repetition rates," Opt. Lett. **41**, 5270 (2016).

27. S. Ou, G. Liu, L. Guo, *et al.*, "870 fs, 448 kHz pulses from an all-polarization-maintaining Yb-doped fiber laser with a nonlinear amplifying loop mirror," Appl. Opt. **57**, 5068 (2018).
28. Y. Liu, G. Liu, Q. Zhao, *et al.*, "140 kHz, 1.2 ps pulses from an all-PM Yb-doped fiber master oscillator-power amplifier," Laser Phys. **31**, 085102 (2021).
29. D. Stoliarov, E. Manuylovich, A. Koviarov, *et al.*, "Gain-managed nonlinear amplification of ultra-long mode-locked fiber laser," Opt. Express **31**, 43427 (2023).
30. Y. Yu, H. Teng, H. Wang, *et al.*, "Highly-stable mode-locked PM Yb-fiber laser with 10 nJ in 93-fs at 6 MHz using NALM," Opt. Express **26**, 10428 (2018).
31. J. Cao, D. Sun, H. Zhuang, *et al.*, "Multiple dissipative soliton Yb-doped fiber laser without an additional filter," Eur. Phys. J. D **75**, 233 (2021).
32. S. Huang, Y. Wang, P. Yan, *et al.*, "Observation of multipulse bunches in a graphene oxide passively mode-locked ytterbium-doped fiber laser with all-normal dispersion," Appl. Phys. B **116**, 939 (2014).
33. E. Kelleher, J. Travers, E. Ippen, *et al.*, "Generation and direct measurement of giant chirp in a passively mode-locked laser," Opt. Lett. **34**, 3526 (2009).
34. R. Woodward, E. Kelleher, T. Runcorn, *et al.*, "Fiber grating compression of giant-chirped nanosecond pulses from an ultra-long nanotube mode-locked fiber laser," Opt. Lett. **40**, 387 (2015).